Image Motion Correction of GATE Simulation in Dedicated PET Scanner with Open Geometry

Héctor Espinós-Morató[1(✉)], David Cascales-Picó[1], Marina Vergara[1,2], and María José Rodríguez-Álvarez[1]

[1] Instituto de Instrumentación para Imagen Molecular (i3M), Universitat Politècnica de València (UPV) - Consejo Superior de Investigaciones Científicas (CSIC), 46022 Valencia, Spain
{hespinos,dcaspic}@i3m.upv.es

[2] Department of Imaging and Pathology, Division of Nuclear Medicine, KU Leuven, 3000 Leuven, Belgium

Abstract. Positron Emission Tomography (PET) images are considerably degraded by respiratory and involuntary motions of the patient inside the scanner, having a direct effect in a misdiagnosis. In this paper, a dedicated PET scanner with an open geometry is proposed. This PET configuration poses several challenges to image reconstruction, such as limited angles, motion correction and the sensitivity correction problem. The paper presents a GATE simulation study of image motion correction using XCAT phantom using a multi-frame algorithm called Enhance Multiple Acquisition Frames (EMAF) to correct rigid body and respiratory motion with list-mode data using time of flight (TOF) information and patient motion. This approach is implemented in three phases: frames cutting, image reconstruction and finally image registration. Additionally, the information provided by the TOF is used to improve the reconstruction due to the lack of angular information provided by the proposed open geometry system. Two performance tests are applied to validate the results, obtaining a remarkable resolution improvement after being processed. The peak signal noise ratio (PSNR) values for the corrected and uncorrected images are, respectively, 30 versus 28 dB, and for the image matching precision (IMP), 89% versus 78%. The obtained results show that the method improves the signal intensity over the background in comparison with other literature methods, maximizing the similarity between the ground-truth (static) image and the corrected image and minimizing the intra-frame motion.

Supported by the Spanish Government Grants TEC2016-79884-C2, PID2019-107790RB-C22, and PEJ2018-002230-A-AR; the Generalitat Valenciana GJIDI/2018/A/040l and the PTA2019-017113-1/AEI/10.13039/501100011033; the European Union through the European Regional Development Fund (ERDF); and the European Research Council (ERC) under the European Union's Horizon 2020 research and innovation program (Grant Agreement No. 695536).

I. Rojas et al. (Eds.): BIOMESIP 2021, LNCS 12940, pp. 3–12, 2021.
https://doi.org/10.1007/978-3-030-88163-4_1

Keywords: Frame-based algorithm · Time of flight · Respiratory motion correction · Non-rigid motion correction · GATE simulation · XCAT phantom · Spatio-temporal registration.

1 Introduction

Organ-dedicated PET systems [1] present some advantages in comparison with conventional or Whole-Body (WB) scanners, i.e., a better spatial resolution and contrast recovery, a higher sensitivity by placing the detectors closer to the organs and a lower cost. The doses of radio-tracer agents injected to the patient is reduced, this makes possible to minimize the radiation exposure, one critical aspect associated to Nuclear Medicine (NM).

In addition, PET scanner explorations tend to put stress on patients (especially those suffering from claustrophobia) [2], who must remain still during the entire scanning process. For these reasons, a dedicated specific open system with modular and optimized geometry that maximizes the angular coverage of the dedicated organ is highly desirable.

Some example of this type of system can be found, e.g. ClearPEM PET [3] or MAMMI PET [4] for breast cancer or ProsPET for prostate cancer [5]; yet, not very common. In this work we present an open PET geometry configuration for an organ-dedicated, where the patient has freedom of movement.

A motion correction strategy based in a framing method present some advantages when compared to other methods. Specifically, joint reconstruction and system matrix modelling present a high computational load in comparison to that of the frame-based methods. In other cases, the system matrix is not available, and the model cannot be applied. Lastly, event rebinning does not allow us to have non-deformable motions such as heartbeat or breathing.

However, despite frame-based motion correction methods presenting a considerable amount of advantages, they also have deficiencies. One of them is the presence of noise in the reconstructed images when motion occurs inside the time duration of a given frame (intra-frame motion). Another example is the image degradation as a consequence of low count statistics that some of the frames can present when the motion is sudden. These deficiencies can affect the clinical practice, where it is necessary to have frames with high statistics and low noise to improve lesion detectability.

In order to overcome the greatest deficiencies of the frame-based algorithms, a novel frame-based motion correction algorithm is proposed in this study. This method is called EMAF (enhanced multiple acquisition frames). The main differences from the original MAF algorithm (multiple acquisition frames developed by Piccard [13]) is that EMAF use of an adaptive threshold in order to divide the original dataset in frames when some prior knowledge of the size of the lesion is present, allowing one to reduce the dose administered to the patient while providing a good, motion-free estimation. It also allows for grouping motions that share similar features under the same frame, thereby increasing the statistics on each frame and reducing the intra-frame motion artefacts. Once the frames are defined, multilevel spatio-temporal registration is performed to ensure a good signal-to-noise ratio.

To summarize, the proposed open PET system poses several challenges to image reconstruction, including (1) a limited angle problem, (2) a motion correction problem, and (3) a sensitivity correction problem.

The paper presents a reconstruction and registration framework to correct rigid and respiratory motion by respiratory gating in list-mode data using time of flight (TOF) information based on a multi-frame algorithm approach based on EMAF algorithm.

2 Materials and Methods

2.1 PET System and GATE Simulation

The PET system was designed [6] with a modular geometry consisting of two panels of 32 × 530 × 353 millimetres with 180 centimetres of separation between them (see Fig. 1). Each panel was formed by 24 modules of 64 LYSO crystals. In order to cover enough angular information, the panels rotates 90 degrees in the longitudinal axis every 5 s.

A 20 s simulation was performed in GATE [7–9] with the XCAT voxelized image [10]. GATE simulation was done with back-to-back gamma particles using a 5 nanoseconds of coincidence window, 10% of blurring resolution and an 350–650 keV energy window.

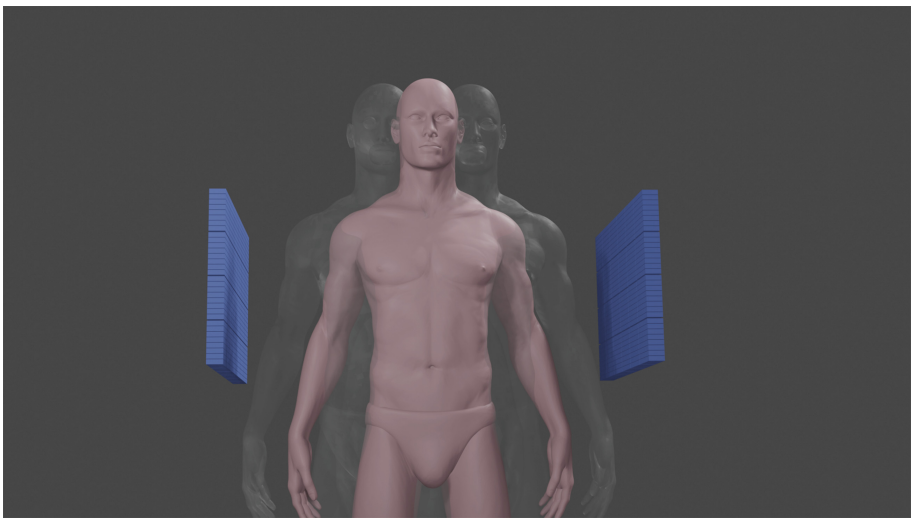

Fig. 1. PET system and a representation of the simulated motion

2.2 XCAT Phantom

XCAT phantom [10] was used to simulate a ^{18}F-FGD scan of a total-body of 1.75 m of height with 1.2 Bq/mm^3 organs activities concentration. The torso

region was cropped afterwards. A lung lesion of 20 millimetres diameter was inserted in the upper lobe of the left lung. The proportion between the lesion to lung contrast was set 4.5:1.

2.3 EMAF Algorithm

Respiratory motion [11] was simulated with a magnitude of 12 millimetres in the anterior-posterior direction and 20 millimetres in the superior-inferior direction. Four cycles of five seconds were reproduced. Additionally, a oscillatory rigid torso-motion in the lateral axis (X) was simulated with the equation $x = Asin(2\pi ft)$ with amplitude (A) of 10 centimetres, and frequency (f) of 0.2 Hz (see Fig. 1).

The presented EMAF algorithm [12] (shown in Fig. 2) is an improved modification based on Picard's original Multiple Acquisition Frames (MAF) Algorithm [13] in order to overcome their most important limitations, such a prefixed number of frames and a short frames with low statistics.

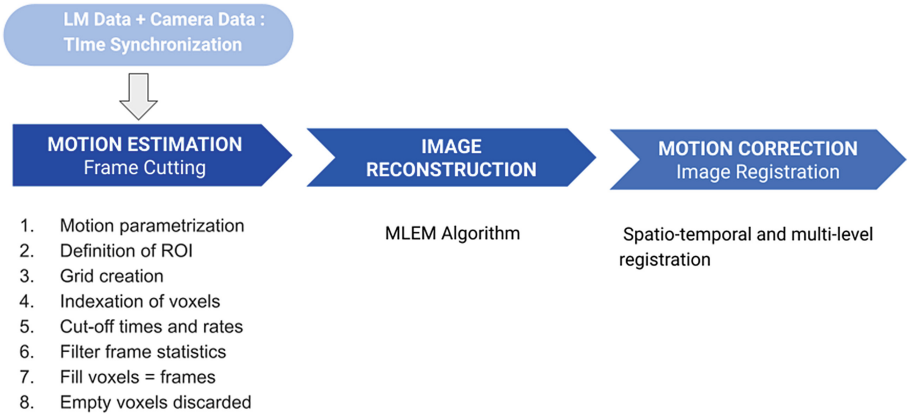

Fig. 2. Proposed algorithm workflow

This method described in detail in [14] consists of three phases. First, the coincidence data given by the PET scanner are divided into different frames following the next steps:

1.- The motion is parametrized by the chosen tracking method. This allows have a 3D motion parametrization in the three directions and angles.

2.- Starting from the previous step, a region of interest (ROI) around the source is defined. This region needs to be wide enough to fit any position recorded by the tracking method. This region will be the grid T.

3.- The ROI is rebinned into an equidistributed and equispaced grid in which the size of each bin (what it defines as voxel) is a free parameter.

4.- Each of the voxels that make up the grid is numbered with an index associated with a certain position in the 3D space. The source motion each moment is stored. This is achieved through two parameters, the time in which the source travels from one voxel to another (called cut-off time) and the index of the voxel (cut-off rates).

5.- In order to apply a time filter, the total time that the source spends in each voxel is calculated. These steps are only followed for those voxels with a total time higher than half the average total voxel time. In this way, using voxels with small statistics that can add noise to the final image is avoided.

6.- For every voxel that passes the aforementioned filter, a new list-mode file is created using the cut-off time and cut-off rate. Once the process has finished, voxels that are completely empty in the grid are discarded.

Coming up next (in the second part of the algorithm), each of those frames are reconstructed separately, and, finally, an spatio-temporal image registration method is performed to align and register the frames into the final reconstructed image.

The approach exposed has two clear advantages: (1) it allows one to group in the same frame motions occurring in the same spatial region, which increases the statistical information; (2) it does not need to prefix a priori the number of possible frames, which allows one to obtain a greater or lesser accuracy depending on the other voxel size of implementation being used.

2.4 Parameter Settings

Once the experimental design carried out has been shown and the steps that make up the movement correction algorithm have been explained, the parameters used in the experimental setting are detailed below.

The algorithm applied for the reconstruction was an iterative Maximum Likelihood expectation maximization [15] with ordered subsets (MLEM-OS).

All the images had a size of $256 \times 256 \times 120$ with pixel size of 1 mm. Five iterations with three subsets were employed for the reconstruction and no corrections were applied.

The motion correction registration EMAF step is a purpose- built subroutine written in C++ and based on the Insight Toolkit (ITK) architecture [16,17]. Spatio-temporal B-spline is applied in a multilevel registration [18], we used a mean square difference (MSD) as the cost function.

The cost function was minimized using gradient descent with 0.01 mm spatial resolution. The optimization is stopped when either a minimal incremental improvement of 0.05 root mean square error (RMSE) value in the cost function is achieved or upon completing 500 rigid iterations plus 300 affine iterations it has been realized (early stop criterion).

One of the points that is taken into account in the development of the registration part is the problem of tissue compression and the partial volume effect (PVE) since they lead to intensity modulations at the same points (pixels) of different reconstructed frames. This effect is usually more visible in thin structures.

In order to avoid image defects caused by intensity variation, we consider the mass preservation property of PET images.

We justify this, taking into account that, when the data are divided into frames, all of them are formed in the same time interval, that is, the entire acquisition time. In other words, in any frame, it is assumed that no radioactivity can be lost or added, apart from some minor changes to the edges of the field of view. For mass preservation, the variational algorithm for mass-preserving image registration (VAMPIRE) algorithm is used [19–23].

Finally, optimization of the multilevel registration algorithm is incorporated. Of first, the algorithm tries to solve discrete optimization at a very coarse level (with a small number of unknowns).

At the time, the approximation transformation is interpolated to the next finer level and used as an initial estimate for minimization of the next objective function.

The procedure is repeated until the transformation is of the desired resolution (user-selected threshold). Consequently, multiple versions of the original images are constructed by iterative downsampling and smoothing of the data.

This procedural scheme has several advantages. First, the likelihood of ending in a local minimum is reduced, as only the main characteristics are taken into account at a certain level. Second, numeric methods, such as that of Gauss–Newton, converge faster for an initial estimate close to the minimum. Third, solving the problems on the coarse grid is computationally more efficient, and, in most cases, only small corrections are required at finer levels.

2.5 Performance Metrics

To validate our corrections two quantitative metrics were used. On the one hand, the Peak Signal to Noise Ratio (PSNR) measured the power of corrupting noise that affects the fidelity of an image representation. Higher values represent a high- quality image.

On the other hand, an Intensity Matching Precision (IMP) test was applied. It measured how deviated the intensities of the moving and fixed images are. A higher IMP value implied a better image matching.

The two metrics have the following expressions:

$$PSNR_{X,F} = 20log_{10}\left(\frac{f_{peak}}{RMSE_{X,F}}\right) \tag{1}$$

$$IMP_{X,F} = \left(1 - \frac{RMSE_{X,F}}{\sqrt{E[F^2]}}\right) \tag{2}$$

where X, F are the moving and fixed images respectively. f_{peak} is the maximum pixel value in the fixed image, and $E[F^2] = \frac{1}{2}\sum_{i=1}^{n} f_i^2$, is the second moment of the fixed image intensity distribution.

3 Results and Discussion

It is proposed a motion correction method of respiratory- gated PET images together with a non-limited patient motion in an open geometry PET system. The experimental results show that spatio-temporal registration has the potential to yield an accurate motion artefacts reduction.

Figure 3 clearly shows that the motion corrected image displays a higher spatial resolution than the uncorrected one. The uncorrected image appears totally blurred, while the lung lesion is conserved in the corrected image. Slight blurring defects were unavoidably found in the image due to lack of lateral information described to the design of our PET system.

The image quality is substantially improved after motion correction using our algorithm, compared to the uncorrected image. The values of PSNR were 30 dB versus 28 dB between static-corrected and static-uncorrected images respectively. The IMP test displayed the same behaviour, with 89% versus 78% between static-corrected and static-uncorrected.

Comparing different experimental designs performed by the proposed motion correction algorithm (EMAF) [14] in closed geometry in comparation with an open planar geometry as described in this manuscript, it can conclude that the results for the Cardio-PET system proposed are relatively good. The results of the EMAF algorithm carried out for closed geometry (ring) give us PSNR values between 37–40 dB, while for CardioPET system, the PSNR result is situated at 30 dB.

If it compared the values of the IMP metric, obviously the values obtained with the application of the motion correction algorithm EMAF are slightly higher for a closed PET geometry (about 90% on average) than for open geometry(89%), due in large part to the loss of angular information mentioned above that the planar PET system shown in the manuscript presents.

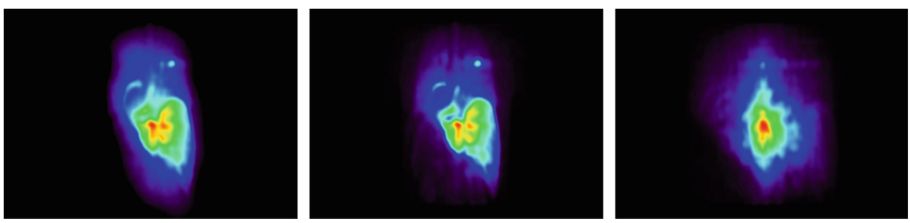

Fig. 3. Reconstruction of the torso-body image (torso with a spherical lesion in the lung). Left to right: static, corrected and uncorrected image. The view is exactly in the same body position of Fig. 1

4 Conclusions

The paper presents a novel motion correction algorithm composed of three phases (motion estimation, image reconstruction, and motion correction). The approach

is based on image registration and frame acquisition of the data. Firstly, the list-mode data obtained from the scanner were sorted into quasi-static frames through a method of cutting into frames consisting of several steps (Fig. 2).

Secondly, each frame was reconstructed using a built in-house MLEM-OS algorithm. Finally, all of the reconstructed frames were registered in order to obtain a final reconstructed image, taking into account that the registration had to be hyperelastic, nonlinear multilevel and spatio-temporal.

Although the number of frames that EMAF produces is minimal, when large spatial motion ranges are present or the structures under study are very small, it produces a high number of frames, which leads to an increase in the computational load.

Despite this limitation, the EMAF algorithm is a robust enhancement that solves the major problems of the original frame-based algorithm and improves the performance of motion correction in a low-intensity range both in closed and opened PET systems.

5 Acronyms

The following acronyms are used in this manuscript displayed in alphabetical order:

EMAF	Enhanced Multiple Acquisition Frames
IMP	Intensity Matching Precision
MLEM-OS	Maximum Likelihood Expectation Maximization with Ordered Subsets
MSD	Mean Square Difference
MAF	Multiple Acquisition Frames
NM	Nuclear Medicine
PSNR	Peak Signal to Noise Ratio
PET	Positron Emission Tomography
RMSE	Root Mean Square Error
ROI	Region Of Interest
TOF	Time of flight
XCAT	4D Extended Cardiac-Torso Phantom
VAMPIRE	Variational Algorithm for Mass-Preserving Image REgistration
WB	Whole-Body

Acknowledgments. This research has been supported by the Spanish Government Grants TEC2016-79884-C2, PID2019-107790RB-C22, and PEJ2018-002230-A-AR; the Generalitat Valenciana GJIDI/2018/A/040l and the PTA2019-017113-1/AEI/10.13039/501100011033; the European Union through the European Regional Development Fund (ERDF); and the European Research Council (ERC) under the European Union's Horizon 2020 research and innovation program (Grant Agreement No. 695536).

Author contributions. Conceptualization: H.E-M. and M.J.R-Á.; methodology: H.E-M.; software: H.E-M., M.V., and D.C-P.; validation: H.E-M. and D.C-P.; formal analysis: H.E-M., D.C-P., and M.V.; investigation, H.E-M., D.C-P., M.V., and Á.H-M.; resources: H.E-M.; data curation, H.E-M., M.V., and D.C-P.; framing: D.C-P.; reconstruction: M.V.; registration: Á.H-M. and H.E-M.; writing—original draft preparation: H.E-M.; writing—review and editing: D.C-P., M.V., Á.H-M., and M.J.R-Á.; visualization: D.C-P. and H.E-M.; supervision: M.J.R-Á.; project administration: M.J.R-Á.; funding acquisition: M.J.R-Á.; J.M.B.B. All authors have read and agreed to the published version of the manuscript.

References

1. González, A.J., Sánchez, F., Benlloch, J.M.: Organ-dedicated molecular imaging systems. In: IEEE Transactions on Radiation and Plasma Medical Sciences, vol. 2, no. 5, pp. 388–403, September 2018. https://doi.org/10.1109/TRPMS.2018.2846745
2. Vaquero, J.J., Kinahan, P.: Positron emission tomography: current challenges and opportunities for technological advances in clinical and preclinical imaging systems. Ann. Rev. Biomed. Eng. **17**, 385–414 (2015). https://doi.org/10.1146/annurev-bioeng-071114-040723
3. Abreu, M.C., et al.: Design and evaluation of the clear-PEM scanner for positron emission mammography. IEEE Trans. Nucl. Sci. **53**(1), 71–77 (2006). https://doi.org/10.1109/TNS.2006.870173
4. Moliner, L., et al.: Design and evaluation of the MAMMI dedicated breast PET. Med. Phys. **39**(9), 5393–5404 (2012). https://doi.org/10.1118/1.4742850
5. Cañizares, G., Gonzalez-Montoro, A., Freire, M., et al.: Pilot performance of a dedicated prostate PET suitable for diagnosis and biopsy guidance. EJNMMI Phys. **7**, 38 (2020). https://doi.org/10.1186/s40658-020-00305-y
6. Oliver, S., Moliner, L., Ilisie, V., Benlloch, J.M., Rodríguez-Álvarez, M.J.: Simulation study for designing a dedicated cardiac TOF-PET system. Sens. (Basel, Switz.) **20**(5), 1311 (2020). https://doi.org/10.3390/s20051311
7. Jan, S., Santin, G., Strul, D., et al.: GATE: a simulation toolkit for PET and SPECT. Phys. Med. Biol. **49**(19), 4543–4561 (2004). https://doi.org/10.1088/0031-9155/49/19/007
8. Jan, S., Benoit, D., Becheva, E., et al.: GATE V6: a major enhancement of the GATE simulation platform enabling modelling of CT and radiotherapy. Phys. Med. Biol. **56**(4), 881–901 (2011). https://doi.org/10.1088/0031-9155/56/4/001
9. Sarrut, D., Bardiès, M., Boussion, N., et al.: A review of the use and potential of the GATE Monte Carlo simulation code for radiation therapy and dosimetry applications. Med. Phys. **41**(6), 064301 (2014). https://doi.org/10.1118/1.4871617
10. Segars, W.P., Sturgeon, G., Mendonca, S., Grimes, J., Tsui, B.M.: 4D XCAT phantom for multimodality imaging research. Med. Phys. **37**(9), 4902–4915 (2010). https://doi.org/10.1118/1.3480985
11. Chan, C., et al.: Non-rigid event-by-event continuous respiratory motion compensated list-mode reconstruction for PET. IEEE Trans. Med. Imaging **37**(2), 504–515 (2018). https://doi.org/10.1109/TMI.2017.2761756
12. Cañizares, G., et al.: Motion correction of multi-frame PET data. IEEE Nuclear Science Symposium and Medical Imaging Conference (NSS/MIC), pp. 1–4 (2019)

13. Picard, Y., Thompson, C.J.: Motion correction of PET images using multiple acquisition frames. IEEE Trans. Med. Imaging **16**, 137–144 (1997). https://doi.org/10.1109/NSS/MIC42101.2019.9059930.Picard
14. Espinós-Morató, H., Cascales-Picó, D., Vergara, M., Hernández-Martínez, Á., Benlloch Baviera, J.M., Rodríguez-Álvarez, M.J.: Simulation study of a frame-based motion correction algorithm for positron emission imaging. Sensors **21**(8), 2608 (2021). https://doi.org/10.3390/s21082608
15. Shepp, L.A., Vardi, Y.: Maximum likelihood reconstruction for emission tomography. IEEE Trans. Med. Imaging **1**(2), 113–122 (1982). https://doi.org/10.1109/TMI.1982.4307558
16. McCormick, M., Liu, X., Jomier, J., Marion, C., Ibanez, L.: ITK: enabling reproducible research and open science. Front. Neuroinf. **2014**(8), 13 (2002). https://doi.org/10.3389/fninf.2014.00013
17. Yoo, T.S., et al.: Engineering and algorithm design for an image processing API: a technical report on ITK – the insight toolkit. In: Westwood, J. (eds.) Proceedings of Medicine Meets Virtual Reality, pp. 586–592. IOS Press Amsterdam (2002)
18. Bai, W., Brady, S.M.: Spatio-temporal image registration for respiratory motion correction in pet imaging. In: Proceedings of the 2009 IEEE International Symposium on Biomedical Imaging: from Nano to Macro, Boston, MA, USA, 28 June–1 July 2009; ISBI 2009, pp. 426–429. IEEE, New York, (2009)
19. Gigengack, F., Ruthotto, L., Burger, M., Wolters, C.H., Jiang, X., Schafers, K.P.: Motion correction in dual gated cardiac PET using mass-preserving image registration. IEEE Trans. Med. Imaging **31**, 698–712 (2012)
20. Arsigny, V., Fillard, P., Pennec, X., Ayache, N.: Fast and simple calculus on tensors in the log-euclidean framework. In: Duncan, J.S., Gerig, G. (eds.) MICCAI 2005. LNCS, vol. 3749, pp. 115–122. Springer, Heidelberg (2005). https://doi.org/10.1007/11566465_15
21. Neumaier, A.: Solving ill-conditioned and singular linear systems: a tutorial on regularization. SIAM Rev. **40**, 636–666 (1998)
22. Burger, M., Modersitzki, J., Ruthotto, L.: A hyperelastic regularization energy for image registration. SIAM J. Sci. Comput. **35**, B132–B148 (2013)
23. Pennec, X.., Stefanescu, R.., Arsigny, V.., Fillard, P.., Ayache, N..: Riemannian elasticity: a statistical regularization framework for non-linear registration. In: Duncan, J.S., Gerig, G. (eds.) MICCAI 2005. LNCS, vol. 3750, pp. 943–950. Springer, Heidelberg (2005). https://doi.org/10.1007/11566489_116